Magnesium-aspartate-based crystallization switch inspired from shell molt of crustacean

Jinhui Tao, Dongming Zhou, Zhisen Zhang, Xurong Xu, and Ruikang Tang[1]

Center for Biomaterials and Biopathways and Department of Chemistry, Zhejiang University, Hangzhou, Zhejiang 310027, China

Edited by James J. De Yoreo, Lawrence Berkeley National Laboratory, Berkeley, CA, and accepted by the Editorial Board November 1, 2009 (received for review August 9, 2009)

Many animals such as crustacean periodically undergo cyclic molt of the exoskeleton. During this process, amorphous calcium mineral phases are biologically stabilized by magnesium and are reserved for the subsequent rapid formation of new shell tissue. However, it is a mystery how living organisms can regulate the transition of the precursor phases precisely. We reveal that the shell mineralization from the magnesium stabilized precursors is associated with the presence of Asp-rich proteins. It is suggested that a cooperative effect of magnesium and Asp-rich compound can result into a crystallization switch in biomineralization. Our in vitro experiments confirm that magnesium increases the lifetime of amorphous calcium carbonate and calcium phosphate in solution so that the crystallization can be temporarily switched off. Although Asp monomer alone inhibits the crystallization of pure amorphous calcium minerals, it actually reduces the stability of the magnesium-stabilized precursors to switch on the transformation from the amorphous to crystallized phases. These modification effects on crystallization kinetics can be understood by an Asp-enhanced magnesium desolvation model. The interesting magnesium-Asp-based switch is a biologically inspired lesson from nature, which can be developed into an advanced strategy to control material fabrications.

biomineralization | calcium biominerals | phase transformation

Biomineralization provides an intelligent strategy to generate functional materials such as mineral skeletons and shells but the understanding of its control mechanism is still a great challenge (1, 2). Different from the conventional solution growth model (3), latest achievements suggest a multistep strategy of phase transformation and highlight the enrollments of transient amorphous precursors in biomineralization (4). Evidences are the first-formed amorphous calcium carbonate (ACC) in sea urchin spicules (5), crustacean cuticles (6), and corals (7), etc. The participations of amorphous calcium phosphate (ACP) in the early stages during tooth and bone generations and the subsequent transformation into carbonated hydroxyapatite (HAP) have been clarified in vivo (8, 9). The precursor role of ACC and ACP in calcium mineralization has also been confirmed in vitro by a number of laboratorial studies (10, 11). It is believed that these amorphous phases are the reservoirs for crystallization and the mechanical strengtheners (4, 10) during biomineral formation. Actually, the pure amorphous calcium minerals are highly unstable in humid environments and therefore, they can hardly be stored in living organisms theoretically. Additives such as magnesium (4, 11, 12), phosphate (11, 13), and macromolecules (10) are involved in the biogenic amorphous phases, acting as the effective stabilizers. However, it is undiscovered how living organisms trigger a rapid crystallization of the temporarily stored precursors to produce the final crystalline biominerals. Although specialized biomolecules have been identified as the regulators of crystal nucleation and growth (3), their functions in modulating phase transformation is rarely evaluated.

In nature, crustacean animals periodically undergo cyclic molt of the exoskeleton, which is essential for their growth, metamorphosis, and reproduction (14–16). *Armadillidium vulgare* belongs to terrestrial-dwelling crustacean taxon isopod. Molt of this animal occurs spontaneously as four typical stages: premolt, intra-molt, postmolt, and inter-molt (6, 14). The layers in cuticle are deposited and mineralized at distinctly different stages (6, 17). That is, calcium ions in old cuticle are resorbed and stored in ACC deposits within the ecdysial gap of the first four anterior sternites in premolt. The crystallization of exocuticle is induced in intra-molt stage (6, 17). The new cuticle forms from the ACC precursors and their crystallization begins with apolysis (separation of hypodermis from existing hard cuticle) and concludes with ecdysis (actual emergence of soft and slimy cuticle). The crystallization in exocuticle is completed in postmolt stage. The endocuticle is calcified in late postmolt several days after ecdysis. A membranous layer is also synthesized during postmolt and its completion signals the onset of inter-molt. During the inter-molt stage, the isopod cuticle can be divided into epicuticle, exocuticle, endocuticle, and membranous layer from outside to inside. The thin epicuticle composes of proteins and possibly long functionalized alkanes (18). Exocuticle is a chitin-protein matrix mineralized with biphase of calcite and ACC (18). Endocuticle is a calcified chitin-protein matrix with only ACC phase. The membranous layer contains chitin and protein but is not calcified (18). Although the phase transformation from ACC into calcite has been suggested during the molt cycle of this species (18), it is unfortunate that we do not know how the living organism controls the crystallization precisely at the desired stage. This unsolved question is actually a key to understanding the biological controls in biomineralization.

Results and Discussion

The spherical particles in sternal deposit is proved to be amorphous (1 in Fig. 1 *A–C*) by the dispersive rings in selected area electron diffraction (SAED) pattern and featureless humps in X-ray diffraction (XRD) pattern. Fourier transform infrared (FT-IR) spectrum (1 in Fig. 1*D*) shows broad and symmetric ν_2 absorption band, 866 cm^{-1}, and split of ν_3 band, 1,475 and 1,420 cm^{-1}, of ACC (4, 10). At early intra-molt stage, the newly formed exocuticle cross-section has many spherical particles of 500 nm in diameter embedded within a porous matrix when imaged in the scanning electron microscopy (SEM) (2 in Fig. 1*B*). Both SAED and FT-IR confirm that these particles are amorphous (2 in Fig. 1 *B* and *D*). However, the weak calcitic peaks in XRD imply that ACC in this stage begins to crystallize (2 in Fig. 1*C*). The obvious transformation of ACC into calcite in exocuticle layer occurs in stage 3 resulting in many calcite crystallites within the organic matrix (3 in Fig. 1*B*), whereas amorphous phase can still be detected in XRD at this stage (3 in Fig. 1*C*). The oriented fusion of the crystallites (4 in Fig. 1*B*) and no

Author contributions: J.T. and R.T. designed research; J.T., D.Z., and Z.Z. performed research; J.T., X.X., and R.T. analyzed data; and J.T. and R.T. wrote the paper.

The authors declare no conflict of interest.

This article is a PNAS Direct Submission. J.J.D. is a guest editor invited by the Editorial Board.

[1]To whom correspondence should be addressed. E-mail: rtang@zju.edu.cn.

This article contains supporting information online at www.pnas.org/cgi/content/full/0909040106/DCSupplemental.

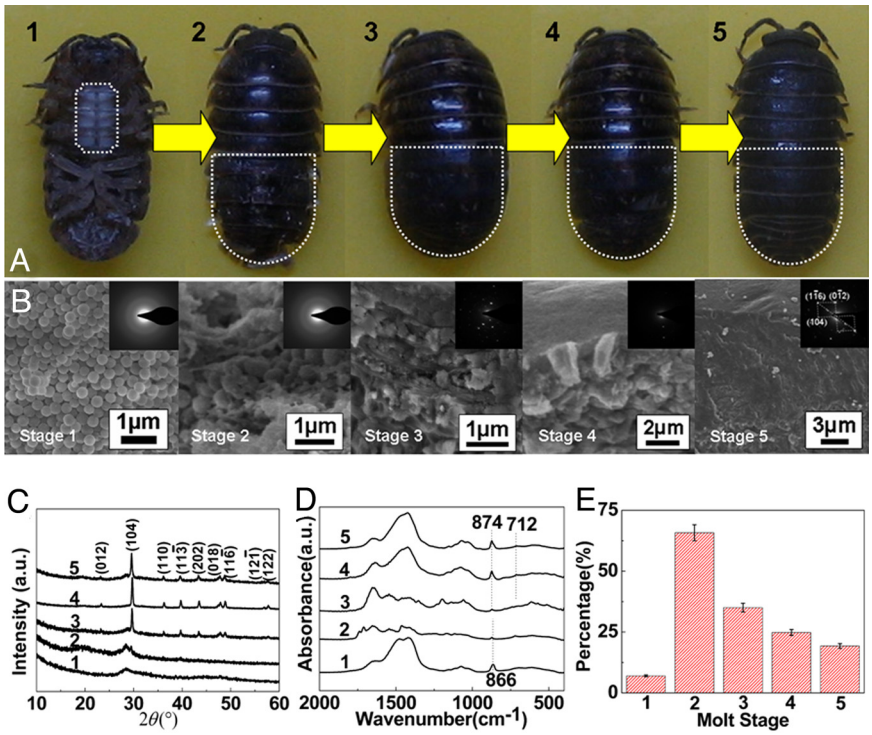

Fig. 1. Morphology, phase, and composition of cuticles at different molt stages. (*A*) Photographs of *Armadillidium vulgare* in the different molt states (1–5). (*B*) SEM images and SAED patterns of the cross-sections of exocuticle layer shown in *A*. (*C* and *D*) XRD patterns and FT-IR spectra, respectively. (*E*) Organic contents of the cuticles during the molt process.

amorphous phase is detected (4 in Fig. 1 *C* and *D*), indicating a complete crystallization within exocuticle in stage 4. In stage 5, the polywood-like chitin-ACC composites of exo- and endocuticle deposit beneath the calcitic layer of exocuticle (Fig. 2), leading to the small amorphous hump in XRD pattern (5 in Fig. 1*C*). The stable ACC phase in stage 5 serves for a mechanical purpose (18) instead of temporary reservoir in stage 1 or as transient precursor in stage 2.

During the shell molt, the stabilities of the ACC phases in the animal are distinct at the different stages, e.g., the ACC is stable

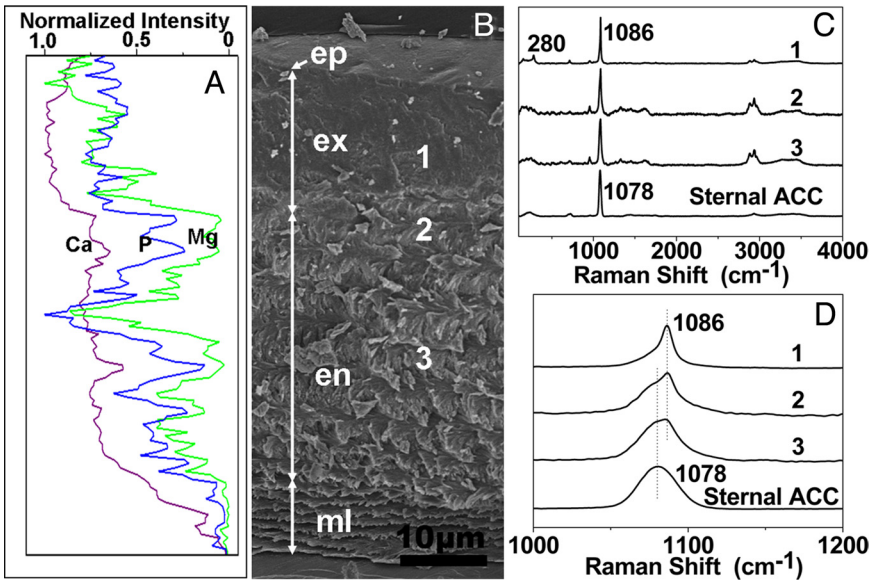

Fig. 2. Structure, element, and phase distribution in an inter-molt cuticle. (*A*) Distribution of Mg, Ca, and P elements in an inter-molt cuticle by electron probe microanalysis corresponding to the cuticle in *B*. (*B*) SEM image of sagittally cleaved fully mineralized cuticle of *Armadillidium vulgare*. The cross-section of cuticle showed the thin epicuticle (ep), calcified exocuticle (ex), and endocuticle (en), and membranous layers (ml). One through three indicate the positions where Raman spectra were collected. (*C*) Raman spectra recorded at corresponding sites indicated in *B*. A spectrum of sternal ACC is used as the reference. Curve 1: exocuticle contained well-crystalline calcite and minor ACC; Curve 2: boundary between exocuticle and endocuticle composed of ACC and minor calcite; Curve 3: endocuticle composed of ACC phase without any detectable calcite. (*D*) A magnified image of spectra in *C*.

in sternites for 1–2 weeks during the premolt period but it can crystallize into calcite within only 8 h in the presence of organic matrix during the intra- and postmolt stages (from 2–4 in Fig. 1*A*). How do the living organisms precisely control the stability of ACC? Actually, the pure amorphous calcium minerals are highly unstable under humid conditions. The molar ratio of Mg/Ca in sternal deposit is 0.02–0.03 estimated by energy dispersive spectroscopy (EDS). Cross-section SEM image shows the layer structure of an inter-molt cuticle (Fig. 2). Distal epicuticle is ≈1-μm in thickness and there is no crystalline phase. Exocuticle is a 15-μm layer with a distal smooth part and a rough transition part. Parallel fibers are visible between the polywood-like stacks and the membranous layer composes loosely stacked plate-like substructures. The phase information of the structured layers is studied by Raman spectroscopy. The bands due to carbonate stretching vibration at 1,086 and 1,078 cm^{-1} are contributed by calcite and ACC, respectively (18). These two phases can also be distinguished by the lattice vibration at 280 cm^{-1} of calcite and a broad band (100–300 cm^{-1}) of ACC (18). It is confirmed that exocuticle mainly consists of calcite (1 in Fig. 2 *C* and *D*). However, ACC and calcite coexist at the boundary between exocuticle and endocuticle (2 in Fig. 2 *C* and *D*). The bands of organic species at 1,321; 1,445; 1,607 cm^{-1} are assigned to the chitin and carboxylate groups in the proteins (18). Endocuticle is constructed by ACC and chitin-protein complex (3 in Fig. 2 *C* and *D*). These results imply that the crystallinities of calcium carbonate minerals are different in the inter-molt cuticle and the organic compounds are involved in the crystallization control. Element distribution map revealed by electron probe microanalysis confirms that the stable ACC in exo- and endocuticle contains relatively high content of Mg than the crystallized zones (Fig. 2*A*). Thus, it is reasonable that the biological stabilization of amorphous phase is attributed to the presence of magnesium (14, 18).

What is the biological signal triggering the crystallization of the temporarily stabilized precursor? Although many extracted proteins associated with mineralized tissue are quite different with species, a common feature is that they contain many acidic moieties and are always rich in aspartic acid (19). The proteins extracted from scleractinian corals, Asp constitutes 40–50 molar percentages (20). In mollusc, Asp usually makes up >50 molar percentages in calcite layers (21). Previous studies have demonstrated that many crustacean exoskeletal proteins are acidic with high contents of Asp and Glu (10, 22).

In our experiments, we find that the main organic component of crustacean cuticle in intra-molt stage is α-chitin (Fig. S1), which is characterized by three characteristic amide bands at 1,657 and 1,628 (amide I), 1,560 (amide II), and 1,313 cm^{-1} (amide III) by FT-IR (23, 24). The spectrum of the soft shell (2 in Fig. 1*D*) shows amide I, a shift of amide II (1,544 cm^{-1}) and the absence of amide III, which may be due to the amide–amide interaction between chitin and some protein backbones. The similar changes in FT-IR have been reported by Falini et al. in their study of chitin-silk fibroin protein interactions (23). Besides, the backbone bands at 1,242 and 1,054 cm^{-1} also indicate the presence of proteins (23). The characteristic absorption band of aspartate at 1,575–1,581 cm^{-1} and carboxylate band at 1,418–1,423 cm^{-1} imply that the involved proteins are rich in acidic residues (25).

We also characterize the organic content during the shell molt by thermogravimetry analysis (TGA) (Fig. 1*E* and Fig. S2). The content of organic species at premolt stage is only approximately 7 wt %. At intra-molt stage, this content increases immediately to approximately 66 wt % and then decreases to ≈35 wt % and approximately 25 wt % in stages 3 and 4, respectively. The organic content in inter-molt is only ≈19 wt %, which is close to a previously reported value, 13 wt % (26). The maximum in organic component coincides with the initiation of phase transformation. Herein, combined with the FT-IR results, it is reasonable to assume that, Asp-rich biomolecules may switch on the crystallization reaction. However, the previous studies of biomimetic mineralization show that Asp-rich peptides and other organic matrices often inhibit crystallization despite that a few of them can accelerate the nucleation at low concentrations (27–30). It is even demonstrated that the cooperation of magnesium and associated proteins can stabilize the amorphous phases more (4, 10, 31). Therefore, only the enhancement effects on the stabilization of amorphous phases (ACC and ACP) by the combination of magnesium and polyelectrolytes (including poly-Asp and poly acrylic acid) have been reported in refs. 32–35. These established understandings are not consistent with some biomineralization phenomena under protein-rich conditions.

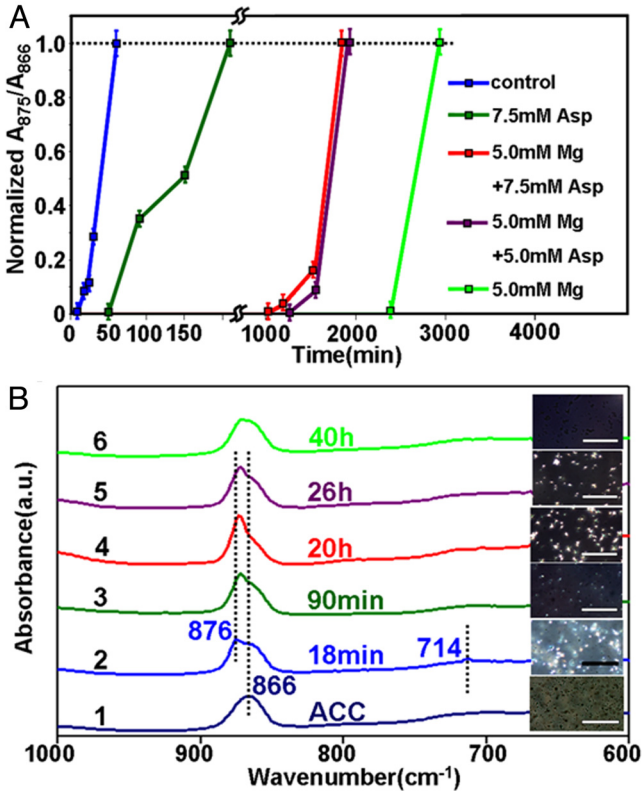

Fig. 3. Kinetics of phase transformation from ACC to calcite. (*A*) Kinetic plot of phase transformation in the absence and presence of magnesium and Asp. (*B*) FT-IR spectra of slightly crystallized samples extracted at different time-scales under different conditions. The inset images are in situ phase evolution investigated by polarizing microscopy in the solvent. (Scale bar, 100 μm.) The calcite and ACC phases are expressed as the bright and dark on the image, respectively. The bright densities can reflect the crystallization degrees during the transition visually.

To examine our assumption, the transformation from ACC to calcite is studied in vitro (Fig. 3*A* and Fig. S3). The crystallization degree of the calcium carbonate is quantitatively estimated by the area ratio between corresponding component ν_2 peaks at 875 cm^{-1} of calcite and 866 cm^{-1} of ACC in FT-IR (Fig. S4*A*). This *ex-situ* method based upon ν_2 symmetry and position is more sensitive than the previous measurement (36, 37), so that it can even monitor poorly crystallized calcium carbonate samples. Polarizing microscopy is also used to monitor the in situ crystals (brilliant domains) nucleation in the bulk solutions. The induction time of phase transformation can be estimated by these two methods complementarily and the results match with each other well (Fig. 3*B*). The crystallization of ACC in pure water is too fast, a mixed solvent containing water and diethylene glycol

(DEG, a model for hydroxyl rich compound chitin) is used as the dispersing media to slow down the crystallization rates. In all experiments, the water/DEG volume ratio is fixed at 0.8, which is close to the reported water content in cuticle of *Armadillidium vulgare*, 40 wt % to 60 wt % (38). In our study, the additives' concentrations are represented by their final concentrations in aqueous component. When the ACC contacts water-DEG, the crystallization of calcite occurs within only approximately 18 min (blue in Fig. 3*A*; Fig. S3 *A* and *B*). However, the spontaneous transformation of ACC in the solvent is effectively switched off; no phase transformation is detected even at 40 h in the presence of 5 mM magnesium (green in Fig. 3*A*, Fig. S3 *E* and *F*). Thus, the lifetime of ACC in the solution is significantly increased so that this unstable phase can be temporarily stored.

Asp is also a stabilizer of ACC phase. The crystallization induction time of ACC is 50 min in the presence of 7.5 mM Asp (olive in Fig. 3*A*; Fig. S3 *C* and *D*). Although Asp poorly inhibits the crystallization of pure ACC, it can switch on the crystallization of the Mg-stabilized ACC. When the same amount of Asp is added into a prestabilized magnesium-ACC system (the concentration of magnesium is maintained at 5 mM), the magnesium-stabilized ACC becomes unstable and the crystallization can be triggered within 17 h (red in Fig. 3*A*; Fig. S3 *G* and *H*). This promotion effect is dose-dependent as the induction time increases to 21 h when the Asp concentration is reduced to 5 mM (purple in Fig. 3*A*; Fig. S3 *I* and *J*). The combination of in situ observation under polarizing microscopy and FT-IR (Fig. 3*B*) demonstrates that the stability of ACC (the transition from ACC to calcite) can be adjustable in a wide range by using magnesium together with Asp.

The similar switch effect can also be observed in another important biomineralization system of calcium phosphates (Fig. 4 and Fig. S5). Splitting function (SF) of calcium phosphate (Fig. S4*B*) proposed by Posner et al. (39) is used as the crystallization indicator due to the characteristic splitting of the phosphate anti-symmetric bending mode (ν_4). Under a buffer aqueous condition, the crystallization of HAP from ACP occurs at 19 min (blue in Fig. 4*A*; Fig. S5 *A* and *B*). This phenomenon indicates that ACP is much more stable than ACC in aqueous environment. Different from the case of calcium carbonate, Asp has no obvious influence on the transformation kinetics from ACP to HAP as the induction time is ≈20 min even when 10 mM Asp is added (olive in Fig. 4*A*; Fig. S5 *C* and *D*). However, the induction time period is >41 h in the presence of 5 mM magnesium (green in Fig. 4*A*; Fig. S5 *E* and *F*). As our expectation, the crystallization of magnesium-stabilized ACP is triggered by 10 mM Asp; the induction time is only approximately 14 h (red in Fig. 4*A*; Fig. S5 *G* and *H*). The crystallization kinetics is accelerated by three times by Asp. The promotion effect of Asp is also dose-dependent in the calcium phosphate phase transformation system. The crystallization from Mg-stabilized ACP to HAP is switched on at ≈24 h when the Asp concentration is 5 mM (purple in Fig. 4*A*; Fig. S5 *I* and *J*). We suggest that the general trends found for magnesium-Asp switch may hold for calcium biomineral formations.

Although Mg or Asp monomer alone can stabilize the amorphous calcium phases, their cooperative effect composes a "crystallization switch" to control the phase transformation in mineralization. It is important to find out why Asp monomer has such an unexpected function. The previous understandings of biomineralization often suggest that polyAsp is an excellent model system to simulate the Asp-rich proteins (33, 34). However, Mann et al. have demonstrated that the polyAsp with long chain-length greatly inhibits ACP transformation while the extracted protein with similar molecular weight promotes the transformation (40). Weiner, Cusack, and their coworkers have also pointed that in the "active sites" of biomineralization proteins, runs of Asp residues commonly separated by either

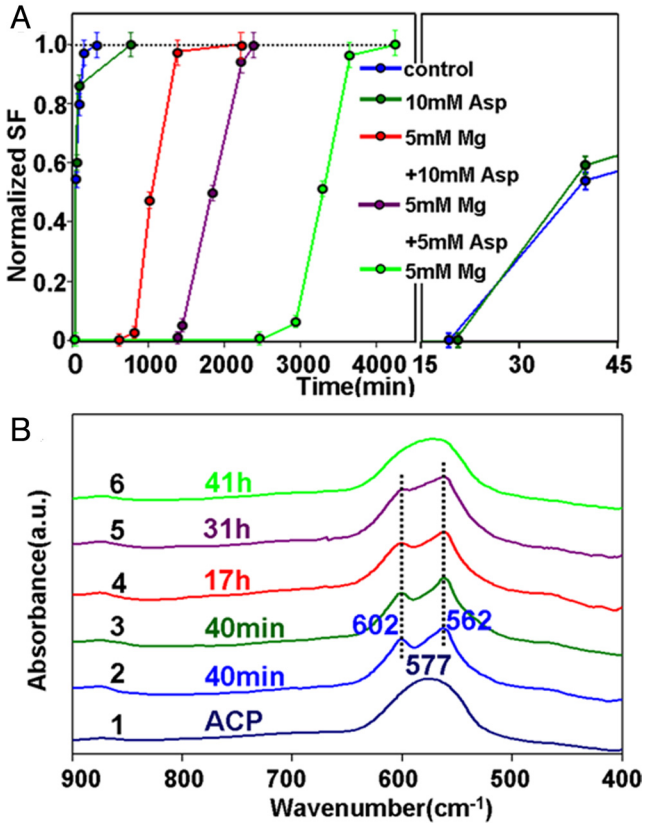

Fig. 4. Kinetics of phase transformation of ACP at different conditions. (*A*) Kinetic plot of phase transformation from ACP to HAP under different conditions. Splitting function (SF) of calcium phosphate is used as the crystallization indicator due to the characteristic splitting of the phosphate anti-symmetric bending mode (*SI Text* and Fig. S5*B*). (*B*) FT-IR spectra of slightly crystallized calcium phosphates extracted at different timescales under different conditions. Pure ACP is used as the reference.

glycine or serine (41, 42). The Asp residues in an acidic block are usually between 1 and 10 units and short polyAsp maybe more common (42). We conclude that polyAsp is in fact distinct from the Asp-rich protein so that polyAsp cannot be considered as a suitable model for the biomineralization proteins. This may be a reason that the switch effect has not been revealed in the previous studies because only the long polyAsp is applied. It is also confirmed experimentally that the short polyAsp segments have a similar role with Asp monomer in the biomimetic studies despite of that the efficiencies may be different (28). Because the function of polyAsp or the other peptides is sensitive to its length (43), the use of Asp monomer is simple and reasonable in the current in vitro model system.

It should be mentioned that the involvement order of magnesium and Asp is also critical to compose the crystallization switch. No switch effect is observed when amorphous phases are first stabilized by Asp, followed by the subsequent addition of magnesium. Therefore, the intelligent biological system may use the inorganic magnesium to switch off and then Asp-rich compounds to switch on the phase transformation. In our in vitro model, the promotion effect of Asp is not so significant as compared with the shell molt of crustacean. However, its tendency of switching on the crystallization of Mg-stabilized amorphous phase is clear. The in vitro study supports the idea about the Mg-biomolecule switch in natural biomineralization. This switch effect induced by Asp is much more important than its promotion degree in the current study. A possible reason for high efficiency may rely on the number of Asp units, charge,

hydrophilicity, and conformation of biomolecules (28, 43). We believe that this biomimetic switch can be improved when the functional "switch on" proteins are applied.

The widespread mechanisms concerning the inhibition of magnesium on crystallization involve mainly two pathways: (*i*) Step "pinning" or "blocking"—the velocity of migrating steps decreases due to magnesium adsorption to step-edges or terraces of calcium mineral and slow dehydration (44, 45). (*ii*) Enhancement of mineral solubility—incorporation of magnesium leads to a lower effective supersaturation of the calcium minerals (46). The previous studies have suggested that the dehydration of cations is the rate-controlling step during the crystallization of ionic crystals (47). The presence of magnesium suppresses the phase transformation of ACC into calcite due to its strong hydration and adsorption onto the surface of incipient nuclei (4, 12, 34, 48). At 25 °C, the enthalpy of dehydration for Mg^{2+} (−1,882 kJ/mol) is greater than that of Ca^{2+} (−1,569 kJ/mol) (49). The dehydration of Mg^{2+} ions before incorporation in the calcite lattice creates an energy barrier to the crystallization of magnesium doped calcium minerals, which may become a rate-limiting step in the phase transformation. There is a possibility that the functional biomolecules can enhance Mg^{2+} desolvation to decrease the dehydration energy barrier. The desolvation of strongly hydrated cations promoted by acidic macromolecules has been reported in calcite growth (28). Dove et al. have also revealed the facilitated magnesium incorporation into magnesium calcite by acidic peptides assisted dehydration effect (50). In this study, Asp may switch on the phase transformation via a similar mechanism. The magnesium contents in calcite are 8.3 ± 0.5 mol % and 13.2 ± 0.8 mol % in the absence and presence of 7.5 mM Asp. It should be noted that the molar ratio of Mg/Ca in the final mineral in the mature cuticle is 0.097 ± 0.002 (Fig. S6*A*), calculated from the shift in (104) peak in XRD using the correlation proposed by Goldsmith et al. (Fig. S6*B*) (51), supporting that the acidic biomolecules enhance magnesium dehydration and incorporation, resulting in the switch on effect.

Besides Asp, another acidic residue, Glu, is also detected in biomineralization proteins (10). In sponges and ascidians, Glu-rich proteins rather than Asp-rich proteins are associated with biogenic ACC (10), while the proteins extracted from the crystalline calcite phases are Asp-rich. It is believed that the Glu-rich proteins together with magnesium are involved in the stabilization of ACC. However, our results suggest that Glu monomer can behave in a manner similar to Asp to accelerate the crystallization of calcium mineralization (Fig. S7*B*). However, such a promotion effect is not detected in the other amino acids, such as Gly and Ala (Fig. S7 *C* and *D*), which confirms the importance of acidic amino acid in biomineralization. This finding is in agreement with the understandings about the acidic proteins in biomineralization studies.

Conclusions

By following the shell molt of crustacean, we confirm that magnesium switches off the phase transformation by stabilizing amorphous precursors and the organic matrices, such as Asp-rich proteins switch on the crystallization by destabilizing the stored amorphous ones. Inspired by this investigation result from living organisms, we use the inorganic magnesium and organic Asp to establish a model system to simulate the crystallization switch in vitro. Both ACC and ACP can be well stabilized by magnesium as the expectation. The subsequent introduction of Asp can effectively switch on the crystallization of these Mg-stabilized amorphous precursors in the laboratory. Such a crystallization control approaches the real biological strategy in the mineral evolutions, which may have a fine perspective in material sciences and chemical biology. The proposed magnesium-Asp-based crystallization switch is another bio-inspired lesson from nature and this discovery provides an understanding of intelligent controls in biomineralization.

Materials and Methods

More detailed descriptions of the experimental procedures, and data analysis are provided in *SI Text*.

Crustacean. The *Armadillidium vulgare* adults (10–14 mm in length) were used in the examinations. The premolt stage was identified by the appearance of white spots at its sternal part. At different molt stages, >30 animals were used for each examination. The excised parts were washed using triple-distilled water for 1–2 s then quickly dehydrated in anhydrous methanol for 1 min. The samples were wiped by a piece of filter paper to remove any remnants of tissue. The cuticles and sternal deposits were dried under a vacuum condition at room temperature for 24 h and then stored at −20 °C. The details of sample preparations are described in *SI Text*.

Calcium Carbonate. ACC was prepared by our laboratory (*SI Text*). ACC was added into DEG at a proportion of 3.95 mg/mL. A volume of 1.6 mL H_2O, $MgCl_2$ (5 mM), and L-Asp (7.5 mM, pH = 8.00) aqueous solutions were added into 1.24 mL DEG to study their individual influence, respectively. A volume of 0.76 mL ACC-DEG slurry was injected into the reaction solutions and the samples were withdrawn periodically. To examine the switch on effect of Asp, 1.36 mL $MgCl_2$ (5.88 mM) aqueous was first added into 0.94 mL DEG. Then 0.76 mL ACC-DEG slurry was injected into the magnesium solution to obtain the magnesium stabilized ACC. At 1 h, 0.54 mL Asp solution was added into the slurry, which was prepared by mixing Asp (50 mM, pH = 8.00) aqueous solution with DEG at the volume ratio of 0.8. The final concentrations of Asp and Mg^{2+} in aqueous component were 7.5 and 5 mM, respectively. We also repeated the experiment at different Asp concentration. The experiments were repeated by using the other amino acids. All of the experiments were performed at 25 °C.

Calcium Phosphate. ACP was synthesized according to our previous method (*SI Text*). The Tris buffer solution (0.15 M, pH = 7.40), buffer with 5 mM $MgCl_2$, and 10 mM Asp were used as the reaction solutions. Five milligrams dried ACP solids were added to the solutions and the transitions were followed by the FT-IR examination of the periodically withdrawn samples. In the switch test, 5 mg ACP powders were added to 4.5 mL buffer containing 5.56 mM Mg^{2+} and 1 h later, 0.5 mL buffer containing Asp (100 or 50 mM) was added. The influences of the other amino acids such as Glu, Ala, and Gly were also examined. All of the transformation experiments were performed at 25 °C.

Characterizations. SEM characterization was performed on S-4800 field-emission scanning electron microscope (HITACHI). FT-IR spectra were collected from 4,000–400 cm^{-1} in transmission mode by a Nexus-670 spectrometer (Nicolet). The transitions from ACC to calcite in solvent were observed by an Eclipse 80i optical microscope (Nikon) in dark field mode. TEM and SAED observations were performed by using CM200UT TEM (Philips). The weight percentage of organic matrix in all biogenic samples were studied by using TGA methods (SDT Q600, TA instrument) performed in a temperature range of 35–800 °C with a heating rate of 10 °C per min in nitrogen atmosphere. The solid phase was examined by XRD (X'PERT PRO, PANalytical) with Cu K_α radiation. Raman spectra of cuticle at different molt stages were recorded at a LabRamHRUV spectrometer (JObin-yvon) operated at a resolution of 4 cm^{-1} with an excitation wavelength of 514 nm.

ACKNOWLEDGMENTS. We thank Dr. J. J. De Yoreo for the constructive discussions and suggestions, Y. D. Xie, H. H. Pan, F. Chen, J. P. Cheng, and Y. W. Wang for their assistances in experiments and characterizations. This work was supported by National Natural Science Foundation of China Grants 20871102 and 20601023, Zhejiang Provincial Natural Science Foundation Grant R407087, and Daming Biomineralization Foundation.

1. Mann S (2001) Biomineralization-principles and concepts in bioinorganic chemistry (Oxford Univ Press, Oxford, UK).
2. Sanchez C, Arribart H, Guille MMG (2005) Biomimetism and bioinspiration as tools for the design of innovative materials and systems. *Nature Mat* 4:277–288.
3. Orme CA, et al. (2001) Formation of chiral morphologies through selective binding of amino acids to calcite surface steps. *Nature* 411:775–779.
4. Addadi L, Raz S, Weiner S (2003) Taking advantage of disorder: Amorphous calcium carbonate and its roles in biomineralization. *Adv Mat* 15:959–970.

5. Politi Y, et al. (2004) Sea urchin spine calcite forms via a transient amorphous calcium carbonate phase. *Science* 306:1161–1164.
6. Dillaman R, Hequembourg S, Gay M (2005) Early pattern of calcification in the dorsal carapace of the blue crab, *Callinectes sapidus. J Morphol* 263:356–374.
7. Meibom A, et al. (2004) Distribution of magnesium in coral skeleton. *Geophys Res Lett* 31:L23306-L23310.
8. Lowenstam HA, Weiner S (1985) Transformation of amorphous calcium phosphate to crystalline dahillite in the radular teeth of chitons. *Science* 227:51–53.
9. Mahamid J, Sharir A, Addadi L, Weiner S (2008) Amorphous calcium phosphate is a major component of the forming fin bones of zebrafish: Indications for an amorphous precursor phase. *Proc Natl Acad Sci USA* 105:12748–12753.
10. Aizenberg J, Lambert G, Weiner S, Addadi L (2002) Factors involved in the formation of amorphous and crystalline calcium carbonate: A study of an ascidian skeleton. *J Am Chem Soc* 124:32–39.
11. Blumenthal NC, Betts F, Posner AS (1977) Stabilization of amorphous calcium phosphate by Mg and ATP. *Calcif Tissue Res* 23:245–250.
12. Raz S, Weiner S, Addadi L (2000) Formation of high-magnesian calcites via an amorphous precursor phase: Possible biological implications. *Adv Mat* 12:38–42.
13. Sawada K (1997) The mechanisms of crystallization and transformation of calcium carbonates. *Pure Appl Chem* 69:921–928.
14. Ziegler A, Fabritius H, Hagedorn M (2005) Microscopical and functional aspects of calcium-transport and deposition in terrestrial isopods. *Micron* 36:137–153.
15. Kuballa AV, Elizur A (2008) Differential expression profiling of components associated with exoskeletal hardening in crustaceans. *BMC Genomics* 9:575.
16. Hecker A. et al. (2004) Orchestin, a calcium-binding phosphoprotein, is a matrix component of two successive transitory calcified biomineralizations cyclically elaborated by a terrestrial crustacean. *J Struct Biol* 146:310–324.
17. O'Brien JJ, Kumari SS, Skinner DM (1991) Proteins of crustacean exoskeletons: I. Similarities and differences among proteins of the four exoskeletal layers of four brachyurans. *Biol Bull* 181:427–441.
18. Hild S, Marti O, Ziegler A (2008) Spatial distribution of calcite and amorphous calcium carbonate in the cuticle of the terrestrial crustaceans *Porcellio scaber* and *Armadillidium vulgare. J Struct Biol* 163:100–108.
19. Weiner S (1979) Aspartic acid-rich proteins: Major components of the soluble organic matrix of mollusk shells. *Calcif Tissue Int* 29:163–167.
20. Mitterer RM (1978) Amino acid composition and metal binding capability of the skeletal protein of corals. *Bull Mar Sci* 28:173–180.
21. Albeck S, Aizenberg J, Addadi L, Weiner S (1993) Interactions of various skeletal intracrystalline components with calcite crystals. *J Am Chem Soc* 115:11691–11697.
22. Sugawara A, et al. (2006) Self-organization of oriented calcium carbonate/polymer composites: Effects of a matrix peptide isolated from the exoskeleton of a crayfish. *Angew Chem Int Ed* 45:2876–2879.
23. Falini G, Weiner S, Addadi L (2003) Chitin-silk fibroin interactions: Relevance to calcium carbonate formation in invertebrates. *Calcif Tissue Int* 72:548–554.
24. Cárdenas G, Cabrera G, Taboada E, Miranda SP (2004) Chitin characterization by SEM, FTIR, XRD, and ^{13}C cross polarization/mass angle spinning NMR. *J Appl Polym Sci* 93:1876–1885.
25. Stankiewicz BA, et al. (1998) Biodegradation of the chitin-protein complex in crustacean cuticle. *Org Geochem* 28:67–76.
26. Becker A, Ziegler A, Epple M (2005) The mineral phase in the cuticles of two species of Crustacea consists of magnesium calcite, amorphous calcium carbonate, and amorphous calcium phosphate. *Dalton Trans* 1814–1820.
27. Fu G, et al. (2005) Acceleration of calcite kinetics by abalone nacre proteins. *Adv Mat* 17:2678–2683.
28. Elhadj S, De Yoreo JJ, Hoyer JR, Dove PM (2006) Role of molecular charge and hydrophilicity in regulating the kinetics of crystal growth. *Proc Natl Acad Sci USA* 103:19237–19242.
29. Tsuji T, et al. (2008) Direct transformation from amorphous to crystalline calcium phosphate facilitated by motif-programmed artificial proteins. *Proc Natl Acad Sci USA* 105:16866–16870.
30. D'Souza SM, et al. (1999) Directed nucleation of calcite at a crystal-imprinted polymer surface. *Nature* 398:312–316.
31. Raz S, et al. (2003) The transient phase of amorphous calcium carbonate in sea urchin larval spicules: The involvement of proteins and magnesium ions in its formation and stabilization. *Adv Funct Mat* 13:480–486.
32. DiMasi E, et al. (2006) Complementary control by additives of the kinetics of amorphous $CaCO_3$ mineralization at an organic interface: In-situ synchrotron X-ray observations. *Phys Rev Lett* 97:045503(1–4).
33. Lam RSK, Charnock JM, Lennie A, Meldrum FC (2007) Synthesis-dependent structural variations in amorphous calcium carbonate. *CrystEngComm* 9:1226–1236.
34. Cheng XG, Varona PL, Olszta MJ, Gower LB (2007) Biomimetic synthesis of calcite films by a polymer-induced liquid-precursor (PILP) process 1. Influence and incorporation of magnesium. *J Cryst Growth* 307:395–404.
35. Ofir PBY, Govrin-Lippman R, Garti N, Füredi-Milhofer H (2004) The influence of polyelectrolytes on the formation and phase transformation of amorphous calcium phosphate. *Cryst Growth Des* 4:177–183.
36. Beniash E, Aizenberg J, Addadi L, Weiner S (1997) Amorphous calcium carbonate transforms into calcite during sea urchin larval spicule growth. *Proc R Soc Lond B* 264:461–465.
37. Gueta R, et al. (2007) Local atomic order and infrared spectra of biogenic calcite. *Angew Chem Int Ed* 46:291–294.
38. Lindqvist OV, Salminen I, Winston PW (1972) Water content and water activity in the cuticle of terrestrial isopods. *J Exp Biol* 56:49–55.
39. Termine JD, Posner AS (1966) Infra-red determination of the percentage of crystallinity in apatitic calcium phosphates. *Nature* 211:268–270.
40. Lévêque I, Cusack M, Davis SA, Mann S (2004) Promotion of fluorapatite crystallization by soluble-matrix proteins from Lingula Anatina shells. *Angew Chem Int Ed* 43:885–888.
41. Weiner S, Hood L (1975) Soluble protein of the organic matrix of mollusk shells: A potential template for shell formation. *Science* 190:987–988.
42. Cusack M, Freer A (2008) Biomineralization: Elemental and organic influence in carbonate systems. *Chem Rev* 108:4433–4454.
43. Elhadj S, et al. (2006) Peptide controls on calcite mineralization: Polyaspartate chain length affects growth kinetics and acts as a stereochemical switch on morphology. *Cryst Growth Des* 6:197–201.
44. Gutjahr A, Dabringhaus H, Lacmann R (1996) Studies of the growth and dissolution kinetics of the $CaCO_3$ polymorphs calcite and aragonite II. The influence of divalent cation additives on the growth and dissolution rates. *J Cryst Growth* 158:310–315.
45. Kanzaki N, et al. (2000) Inhibitory effect of magnesium and zinc on crystallization kinetics of hydroxyapatite (0001) face. *J Phys Chem B* 104:4189–4194.
46. Davis KJ, Dove PM, De Yoreo JJ (2000) The role of Mg^{2+} as an impurity in calcite growth. *Science* 290:1134–1137.
47. Reddy MM, Nancollas GH (1971) The crystallization of calcium carbonate: I. isotopic exchange and kinetics. *J Colloid Interface Sci* 36:166–172.
48. Loste E, Wilson RM, Seshadri R, Meldrum FC (2003) The role of magnesium in stabilising amorphous calcium carbonate and controlling calcite morphologies. *J Cryst Growth* 254:206–218.
49. Huheey JE (1983) Inorganic Chem: Principles of Structure and Reactivity (Harper and Row, New York) 3rd Ed.
50. Stephenson AE, et al. (2008) Peptides enhance magnesium signature in calcite: Insights into origins of vital effects. *Science* 322:724–727.
51. Goldsmith JR, Graf DL, Heard HC (1961) Lattice constants of the calcium-magnesium carbonates. *Am Mineral* 46:453–457.